



1 **Modeling of non-structural carbohydrate dynamics by the spatially**  
2 **explicitly individual-based dynamic global vegetation model SEIB-**  
3 **DGVM (SEIB-DGVM-NSC ver1.0)**

4  
5 **Hideki Ninomiya<sup>1</sup>, Tomomichi Kato<sup>2</sup>, Lea Végh<sup>2</sup>, and Lan Wu<sup>3</sup>**

6  
7 <sup>1</sup>Graduate School of Global Food Resources, Hokkaido University, Sapporo, Hokkaido 060-0809,  
8 Hokkaido, Japan

9 <sup>2</sup>Research Faculty of Agriculture, Hokkaido University, Sapporo, Hokkaido 060-8589, Japan

10 <sup>3</sup>College of Ecology and Environment, Hainan University, Hainan, China

11

12 **Correspondence:** Tomomichi Kato (tkato@cen.agr.hokudai.ac.jp)

13 Tel & Fax: +81 11 706 4942

14

15 **Abstract.** Forest dynamics need to be considered when estimating the global carbon budget. The  
16 alteration of forest structure and function under a changing climate and expanding human activity  
17 could lead to a reduction of forest canopy cover and a spread of lower-biomass ecosystems in  
18 warm and dry regions. Non-structural carbohydrate (NSC) acts as a storage buffer between carbon  
19 supplied by assimilation and carbon consumed by, inter alia, respiration, reproduction, and pests.  
20 Estimation of NSC concentrations in a tree is very important for accurate projection of future  
21 forest dynamics. We developed a new NSC module for incorporation into a spatially explicit,  
22 individual-based, dynamic global vegetation model (SEIB-DGVM) to validate the simulated NSC  
23 dynamics with observations. NSC pools were simulated in three plant organs: leaves, trunk, and  
24 roots. The seasonal dynamics of the NSCs varied among plant species, and the sizes of the NSC  
25 pools inferred from observations differed between the boreal, temperate, and tropical climates.  
26 The NSC models were therefore validated for each of the three climatic regions at both point and  
27 global scales to assess the performance of the models. The modeled NSCs showed good  
28 agreement in seasonality with the observed NSCs at four sites—Canada (boreal), Austria and  
29 Switzerland (temperate), and Panama (tropical)—and in mean values for three climate zones  
30 derived from the global NSC dataset. The SEIB-DGVM-NSCv1.0 is expected to enable  
31 simulation of biome shifts caused by the changes of NSC dynamics worldwide. These dynamics  
32 will contribute to changes of not only the global carbon cycle but also of forest structure and  
33 demography at a global scale.

34

35



## 36 **1 Introduction**

37

38 Permanent shifts in forest vegetation dynamics have already been observed and are expected to  
39 accelerate under future changes of climate globally (McDowell et al., 2020). Forest dynamics are  
40 changing due to anthropogenic drivers, such as rising temperatures and CO<sub>2</sub> partial pressures, and  
41 are affected by transient disturbances such as wildfires, droughts, biotic attacks, and land-use  
42 changes. The dependence of tree recruitment and growth on spatial and temporal drivers could  
43 lead to an increase of tree mortality rates in warm and dry regions (Stevens-Rumann et al., 2018;  
44 Xu et al., 2017). These changes will cause forests to become shorter and younger. The result will  
45 be a net reduction of forest canopy cover and a shift toward low-biomass ecosystems. Furthermore,  
46 higher tree mortality will have a negative impact on global ecosystem: lower biological diversity,  
47 a decrease of wild animal habitat, altered hydrological and carbon cycles, and increased  
48 vulnerability to sudden invasions by exotic species (Adams et al., 2013). Understanding the  
49 drivers of vegetation dynamics requires accurately simulating the effect of climate change on  
50 global terrestrial biogeochemistry.

51 To increase their chance of survival, trees control their carbon resources and strategically  
52 allocate them to growth, respiration, storage, reproduction, and defense (Hoch et al., 2003;  
53 Hartmann et al., 2018). When the atmospheric partial pressure of CO<sub>2</sub> increases, trees can allocate  
54 surplus carbon to either growth or carbon storage (Hoch et al., 2003; Huang et al., 2020). Changes  
55 in tree carbon allocation patterns have been shown to exert large effects on constituents of the  
56 terrestrial carbon cycle (Klein and Hoch, 2015). Clarification of the importance of carbon  
57 allocation has revealed that non-structural carbohydrates (NSCs) draw much from the other  
58 carbon resources because they are the most significant carbon compounds involved in the life  
59 processes of trees (He et al., 2020).

60 The NSC is comprised of starch and sugars, which are mobilized mainly for growth and  
61 metabolism when little recently assimilated carbon is available (Gough et al., 2010; Richardson  
62 et al., 2013; Chuste et al., 2020; Herrera-Ramírez et al., 2020). During photosynthesis, freshly  
63 assimilated carbon is transported as triose phosphate from the chloroplast to the cytosol, where  
64 sucrose is synthesized from it. Some of the sucrose is then changed into starch in the chloroplast,  
65 and the starch is consumed to maintain growth and metabolism at times when recently assimilated  
66 carbon is not available to the plants (Dietze et al., 2014). Plants that seasonally shed leaves need  
67 to rely on stored carbon for maintenance during the leafless season. NSCs play an important role  
68 as substrates for the synthesis of compounds in plants and as energy sources for metabolic  
69 activities (Hartmann et al., 2018). Moreover, NSCs include key compounds that are used to buffer  
70 physiological stress when energy from photosynthesis does not satisfy metabolic demands  
71 (Gough et al., 2010; Sala et al., 2012) because carbohydrates such as starch can be easily



72 mobilized and reallocated (Hartmann et al., 2018).

73 In long-lived plants, the ability to store carbon is a key to survival at times when  
74 photosynthetic rates are low because of shade, drought, and disturbance (Martínez-Vilalta et al.,  
75 2016). As a result, **the amount of NSC depends** on the balance between the supply and demand of  
76 assimilated carbon and accounts for a large fraction of the annual carbon budget of plants  
77 (Richardson et al., 2013). When carbon allocation patterns favor storage over growth, tree growth  
78 is limited (Wang et al., 2021). Hence, the dynamics of stored carbon pools can be considered an  
79 indicator of the carbon balance of the plant.

80 Because the frequency, duration, and severity of droughts are expected to increase globally,  
81 the damage to plants through rising temperatures, water vapor pressure **deficiency**, and associated  
82 water loss will also increase (IPCC, 2014; Sevanto and Dickman, 2015). Trees **are** killed directly  
83 by **drought** or indirectly by associated increases of insect or pathogen attacks. Indirect effects that  
84 cause tree **mortalities** include girdling of the phloem **and xylem** by bark beetles and defoliation  
85 events that delay **recovery of trees**. The frequency and severity of this indirect biotic disturbance  
86 from insects and insect–pathogen complexes have been increasing (McDowell et al., 2020; Seidl  
87 et al., 2017). According to multiple observational and experimental studies, the resulting  
88 imbalance between NSC demand and **supply leads to carbon starvation**, which is one of the  
89 mechanisms that contribute to drought-induced mortality (McDowell, 2011).

90 The decline of stomatal conductance during a drought reduces photosynthetic carbon  
91 assimilation and thus decreases the amount of NSC (McDowell et al., 2008; Adams et al., 2017).  
92 Although an imbalance of the NSC pool could mechanistically trigger plant mortality, few  
93 ecological models predict tree mortality resulting from the role of NSC associated with climate  
94 change (Adams et al., 2013; McDowell, 2011). Simulations of the NSC dynamics of plants will  
95 elucidate the effects of different drivers on forested ecosystems (Gough et al., 2010).

96 Dynamic global vegetation models (DGVMs) are often used to represent vegetation dynamics  
97 as well as biogeochemical cycles and to simulate the transition of the vegetation structure in  
98 response to climatic changes via modeling of competition and disturbance (Hickler et al., 2004;  
99 Krinner et al., 2005; Braakhekke et al., 2019). In DGVMs, plant species are classified into plant  
100 functional types (PFTs) based on their eco-physiological traits. However, most DGVMs  
101 oversimplify individual plant competition by using average values of traits for each PFT (Smith  
102 et al., 2001). Most of such models miss the effects of local competition for light, which must be  
103 considered when modeling gap population dynamics among individual trees (Sato et al., 2007).

104 In contrast, the Spatially Explicit, Individual-Based, Dynamic Global Vegetation Model  
105 (SEIB-DGVM; Sato et al., 2007) can simulate the growth of individual trees on numerous  
106 replicate patches and enable observation of how single, large trees can influence nearby trees.  
107 Plants in different patches do not interact with each other in terms of physical resources such as



108 light and water. In each patch, **the growth, competitive interactions, and mortality of each tree are**  
109 **calculated based on environmental conditions.** Transient changes in vegetation distribution and  
110 dynamics can therefore be examined (Sato et al., 2007).

111 SEIB-DGVM has been used to simulate a transient change in the distribution and function of  
112 vegetation on the African continent in conjunction with the ranges of dispersal of trees and to  
113 address factors that had a strong impact on the transient change (Sato and Ise, 2012). Use of the  
114 SEIB-DGVM has enabled reconstruction of the geographical distributions of plant productivity  
115 and thermo-hydrology based on observations in eastern Siberia and partial representation of the  
116 effect of topography on the abundance of trees in larch forests (Sato et al., 2020). The SEIB-  
117 DGVM was coupled with a **flagship** Earth system model (MIROC-ESM; Watanabe et al., 2011).  
118 Because the amount of stored NSC depends on the size of individual trees and because the SEIB-  
119 DGVM can simulate individual trees, we chose the SEIB-DGVM to estimate the NSC dynamics  
120 of plants.

121 The objectives of the research were to 1) incorporate a module to **simulate NSC dynamics** in  
122 the SEIB-DGVM and 2) validate the simulated NSC dynamics with observational data at both  
123 point and global scales. We therefore created a new function in the SEIB-DGVM to represent the  
124 NSC dynamics of individual trees. How NSC is produced, stored, and distributed among different  
125 plant organs under environmental stress is poorly understood (Jones et al., 2019; Rademacher  
126 et al., 2021; Wang et al., 2021). Our enhanced model improves the physiological simulation of the  
127 leaf life cycle and enhances understanding of how NSC affects the distribution of vegetation,  
128 gross primary production (GPP), net primary production (NPP), and carbon stocks as well as tree  
129 dynamics (age, height, and trunk diameter) at global scales in the future. By adjusting the NSC  
130 accumulation rates of individual trees and the threshold of NSC-induced mortality during drought,  
131 the model can simulate the timing, location, and percentage of trees that die in response to  
132 moderate drought. Furthermore, the model can increase our understanding of the role of carbon  
133 **reserves.**

134

## 135 **2 Model**

136

### 137 **2.1 Spatially Explicit Individual-Based Dynamic Global Vegetation Model (SEIB-DGVM)**

138

139 The SEIB-DGVM (v3.02; [http://seib-dgvm.com/data/seib\\_code302.zip](http://seib-dgvm.com/data/seib_code302.zip); Sato et al., 2016) is a  
140 carbon budget model that simulates the establishment of individual trees, competition between  
141 trees, and the death of individual trees according to input climate data. The default settings follow  
142 the structure of a three-dimensional virtual forest on a 30 m × 30 m stand of trees with 1 m × 1 m  
143 simulation grid cells. In each grid cell, a tree belonging to one of 14 woody plant functional types



144 (PFTs) is assigned **if** conditions allow in addition to one of 2 grass PFTs. All physical and  
 145 physiological processes are calculated at daily time steps, trunk growth is estimated monthly, and  
 146 vegetation dynamics and **disturbance** are assessed annually. Because of the lack of field  
 147 observations at the time the model was developed, there is no mechanism to control the **carbon**  
 148 **stock in leaves and roots** in the original SEIB-DGVM, and only the carbon stock in trunks is  
 149 simulated after adjusting the available organic matter for reproduction and respiration. The  
 150 original SEIB-DGVM therefore cannot represent carbon starvation **effectively** without accounting  
 151 for the carbon stock in leaves and roots, **even though the carbon stock of the trunk depends on the**  
 152 **leaf mass from the previous day.**

153

## 154 2.2 NSC components

155

### 156 2.2.1 NSC pool

157 The new **NSC pools** are separated into three organs of an individual tree: leaves, trunk, and roots.  
 158 The original SEIB-DGVM simply allocates the surplus carbon that remains after respiration for  
 159 the growth of roots and then, if more than 30 days have passed since foliation, for the **growth of**  
 160 **leaves** and the trunk. In this study, the carbon newly assimilated via photosynthesis goes into three  
 161 NSC pools. The NSC pools can be later mobilized for growth and respiration as follows (Fig. 1).

162

$$163 \Delta NSC_t = NPP_t = \Delta NSC_{trunk,t} + \Delta NSC_{leaf,t} + \Delta NSC_{root,t}, \quad (1)$$

164

165 when  $NSC_{trunk,t-1} < NSC_{trunk,max(t)}$ ,  $NSC_{leaf,t-1} < NSC_{leaf,max(t)}$ , and  $NSC_{root,t-1} < NSC_{root,max(t)}$ ,

166

$$167 \begin{cases} \text{parent } NSC_{trunk,t} = \min(NSC_{trunk,max(t)}, \Delta NSC_t), \\ NSC_{leaf,t} = \min(NSC_{leaf,max(t)}, \Delta NSC_t - NSC_{trunk,t}), \\ NSC_{root,t} = \min(NSC_{root,max(t)}, \Delta NSC_t - NSC_{trunk,t} - NSC_{leaf,t}), \end{cases} \quad (2)$$

168

169 when  $NSC_{trunk,t-1} < NSC_{trunk,max(t)}$ ,  $NSC_{leaf,t-1} < NSC_{leaf,max(t)}$ , and  $NSC_{root,t-1} > NSC_{root,max(t)}$

170

$$171 \begin{cases} NSC_{trunk,t} = \min(NSC_{trunk,max(t)}, \Delta NSC_t), \\ NSC_{leaf,t} = \min(NSC_{leaf,max(t)}, \Delta NSC_t - NSC_{trunk,t}), \\ NSC_{root,t} = NSC_{root,max(t)} \end{cases}, \quad (3)$$

172

173 when  $NSC_{trunk,t-1} < NSC_{trunk,max(t)}$ ,  $NSC_{leaf,t-1} > NSC_{leaf,max(t)}$ , and  $NSC_{root,t-1} < NSC_{root,max(t)}$ ,

174



$$\begin{cases}
 \text{NSC}_{\text{trunk},t} = \min(\text{NSC}_{\text{trunk},\text{max}(t)}, \Delta \text{NSC}_t), \\
 \text{NSC}_{\text{leaf},t} = \text{NSC}_{\text{leaf},\text{max}(t)}, \\
 \text{NSC}_{\text{root},t} = \min(\text{NSC}_{\text{root},\text{max}(t)}, \Delta \text{NSC}_t - \text{NSC}_{\text{trunk},t} - \text{NSC}_{\text{leaf},t}),
 \end{cases} \quad (4)$$

176

177 when  $\text{NSC}_{\text{trunk},t-1} < \text{NSC}_{\text{trunk},\text{max}(t)}$ ,  $\text{NSC}_{\text{leaf},t-1} > \text{NSC}_{\text{leaf},\text{max}(t)}$ , and  $\text{NSC}_{\text{root},t-1} > \text{NSC}_{\text{root},\text{max}(t)}$ ,

178

$$\begin{cases}
 \text{parent NSC}_{\text{trunk},t} = \min(\text{NSC}_{\text{trunk},\text{max}(t)}, \Delta \text{NSC}_t), \\
 \text{NSC}_{\text{leaf},t} = \text{NSC}_{\text{leaf},\text{max}(t)}, \\
 \text{NSC}_{\text{root},t} = \text{NSC}_{\text{root},\text{max}(t)},
 \end{cases} \quad (5)$$

180

181 when  $\text{NSC}_{\text{trunk},t-1} > \text{NSC}_{t,\text{max}(t)}$ ,  $\text{NSC}_{\text{leaf},t-1} < \text{NSC}_{\text{leaf},\text{max}(t)}$ , and  $\text{NSC}_{\text{root},t-1} < \text{NSC}_{\text{root},\text{max}(t)}$ ,

182

$$\begin{cases}
 \text{NSC}_{\text{trunk},t} = \text{NSC}_{t,\text{max}(t)} \\
 \text{NSC}_{\text{leaf},t} = \min(\text{NSC}_{\text{leaf},\text{max}(t)}, \Delta \text{NSC}_t), \\
 \text{NSC}_{\text{root},t} = \min(\text{NSC}_{\text{root},\text{max}(t)}, \Delta \text{NSC}_t - \text{NSC}_{\text{trunk},t} - \text{NSC}_{\text{leaf},t}),
 \end{cases} \quad (6)$$

184

185 when  $\text{NSC}_{\text{trunk},t-1} > \text{NSC}_{t,\text{max}(t)}$ ,  $\text{NSC}_{\text{leaf},t-1} < \text{NSC}_{\text{leaf},\text{max}(t)}$ , and  $\text{NSC}_{\text{root},t-1} > \text{NSC}_{\text{root},\text{max}(t)}$ ,

186

$$\begin{cases}
 \text{NSC}_{\text{trunk},t} = \text{NSC}_{t,\text{max}(t)}, \\
 \text{NSC}_{\text{leaf},t} = \min(\text{NSC}_{\text{leaf},\text{max}(t)}, \Delta \text{NSC}_t), \\
 \text{NSC}_{\text{root},t} = \text{NSC}_{\text{root},\text{max}(t)},
 \end{cases} \quad (7)$$

188

189 when  $\text{NSC}_{\text{trunk},t-1} > \text{NSC}_{t,\text{max}(t)}$ ,  $\text{NSC}_{\text{leaf},t-1} > \text{NSC}_{\text{leaf},\text{max}(t)}$ , and  $\text{NSC}_{\text{root},t-1} < \text{NSC}_{\text{root},\text{max}(t)}$ ,

190

$$\begin{cases}
 \text{NSC}_{\text{trunk},t} = \text{NSC}_{t,\text{max}(t)}, \\
 \text{NSC}_{\text{leaf},t} = \text{NSC}_{\text{leaf},\text{max}(t)}, \\
 \text{NSC}_{\text{root},t} = \min(\text{NSC}_{\text{root},\text{max}(t)}, \Delta \text{NSC}_t),
 \end{cases} \quad (8)$$

192

193 when  $\text{NSC}_{\text{trunk},t-1} > \text{NSC}_{t,\text{max}(t)}$ ,  $\text{NSC}_{\text{leaf},t-1} > \text{NSC}_{\text{leaf},\text{max}(t)}$ , and  $\text{NSC}_{\text{root},t-1} > \text{NSC}_{\text{root},\text{max}(t)}$ ,

194

$$\begin{cases}
 \text{NSC}_{\text{trunk},t} = \text{NSC}_{t,\text{max}(t)}, \\
 \text{NSC}_{\text{leaf},t} = \text{NSC}_{\text{leaf},\text{max}(t)}, \\
 \text{NSC}_{\text{root},t} = \text{NSC}_{\text{root},\text{max}(t)},
 \end{cases} \quad (9)$$

196

197 where  $t$  is the calculation day,  $t-1$  is the previous day,  $\text{NSC}_{\text{organ}}$  is the amount of NSC in each organ,

198 and  $\text{NSC}_{\text{organ},\text{max}(t)}$  is the maximum amount of NSC in each organ on day  $t$ .



199 First, the surplus carbon that remains after respiration is assigned to the NSC trunk pool using  
 200 Eq. (1). As long as the trunk biomass increases relative to that on the previous day, the **overflowing**  
 201 **carbon** moves primarily into NSC<sub>leaf</sub>, secondarily into NSC<sub>root</sub>, and finally into the growth of  
 202 leaves, the trunk, and roots. The sum of the NSCs in the leaves, trunk, and roots (the total NSC)  
 203 is **maximized** for each climate region (Table 1). If the total NSC exceeds this upper limit, the  
 204 surplus is directly consumed for the growth of each organ.

205

206

**Table 1.** Maximum **volume** of NSC pool

Maximum of NSC pool		
Boreal	10% of total biomass	Martínez-Vilalta et al. (2016)
Temperate	5% of total biomass	Hoch et al. (2003)
Tropical	9% of total biomass	Würth et al. (2005)

207

208 The NSC pools of the organs displays unique seasonality for each climatic zone. The NSC  
 209 seasonality of each organ varies among tree species mainly because the climate and surrounding  
 210 environment influence the capacity and utilization of NSCs in plants. To take into consideration  
 211 the fact that field observations of NSC **covered whole seasons** and that various plant species were  
 212 scarce, we classify NSC seasonality into three types: tropical, temperate, and boreal. Observations  
 213 from temperate forests showed that the NSC seasonal cycles were similar among the organs and  
 214 peaked around late spring–summer, although the NSC<sub>organ</sub> differed in size (Hoch et al., 2003;  
 215 Richardson et al., 2013; Woodruff and Meinzer, 2011; Gruber et al., 2012). In contrast, the NSC  
 216 concentrations in the leaves of boreal trees peak in June (Sveinbjörnsson et al., 2010), and NSCs  
 217 in the fine roots increase until summer and then decline toward mid-summer and fall because of  
 218 the initiation of root growth (Landhäusser and Lieffers, 2003). All 14 woody PFTs of the SEIB-  
 219 DGVM are sorted into one of **three NSC types**, and carbon assimilated via photosynthesis was  
 220 allocated to the NSC pool of each organ in temperate and boreal PFTs as follows.

221

$$222 \text{NSC}_{\text{organ, max}} = (a + b \times \text{daily GPP}) \times \text{Biomass}, \quad (10)$$

223

224 where the organ is either a leaf, trunk, or root, *a* is the minimum value, and *b* is the seasonality  
 225 parameter.

226

227 Tropical species have a different NSC seasonality from temperate and boreal species. The  
 228 NSC of leaves display a concave upward seasonal pattern that reaches its minimum in late spring–  
 229 early summer (Würth et al., 2005), which is a dry season when leaf production and flowering  
 229 deplete NSC pools. Singh and Srivastava (1986) have observed that the NSC of roots is at a  
 230 minimum level from July to September because the NSC pool is drained to enable survival of the



231 rainy season during that period. The amount of NSCs then increases toward winter, when the fine  
 232 root biomass declines. Hence, Eq. (10), which is used for temperate and boreal forests, is  
 233 inadequate for simulation of tropical forests because the NSC depends less on the seasonality of  
 234 photosynthesis in the tropics. The size of the NSC pool of tropical species therefore accumulates  
 235 as follows.

236

$$237 \text{NSC}_{\text{organ, max}} = (a + b) \times \text{Biomass}, \quad (11)$$

238

239 where the organ is either the leaf, trunk, or root,  $a$  is the minimum value, and  $b$  is the seasonality  
 240 parameter.

241

## 242 2.2.2 NSC expenditure

243

### 244 2.2.2.1 Respiration

245

246 Normally, photosynthetically assimilated carbon is used for maintenance respiration without  
 247 entering the carbon storage system. When the **assimilated carbon is inadequate** for maintenance  
 248 respiration, the **NSC** compensates for the shortage. The NSC **loss is allocated** to each organ as  
 249 follows.

250

$$251 \text{NSC}_{\text{leaf, t}} = \text{NSC}_{\text{leaf, t-1}} - R_{a, t-1} \times c_{\text{leaf}} \quad (12)$$

$$252 \text{NSC}_{\text{trunk, t}} = \text{NSC}_{\text{trunk, t-1}} - R_{a, t-1} \times c_{\text{trunk}} \quad (13)$$

$$253 \text{NSC}_{\text{root, t}} = \text{NSC}_{\text{root, t-1}} - R_{a, t-1} \times c_{\text{root}}, \quad (14)$$

254

255 where autotrophic respiration ( $R_a$ ) is the difference between assimilated carbon and maintenance  
 256 respiration and  $c$  is the allocation factor for NSC utilization ( $c_{\text{leaf}} + c_{\text{trunk}} + c_{\text{root}} = 1$ ). If the total  
 257 NSC equals the carbon shortfall, the NSC of all organs becomes zero. The allocation factors of  
 258 NSC utilization depend on the climatic region (Table 2). If an  $\text{NSC}_{\text{organ}}$  is inadequate to provide  
 259 the allocated share of  $R_a$ , the other organs will supply the difference: the  $\text{NSC}_{\text{leaf}}$  is supplemented  
 260 first from the  $\text{NSC}_{\text{trunk}}$ , and if that is not enough, from the  $\text{NSC}_{\text{root}}$ . Similarly, if any of the other  
 261  $\text{NSC}_{\text{organ}}$  pools is unable to cover local shortages, the NSC pools of the remaining organs will  
 262 balance the supply and demand.

263

264

**Table 2.** Allocation ratio ( $c$ ) of NSC to organs

Organ	Boreal	Temperate	Tropical
Leaf	<b>0.20</b>	0.05	0.01





Trunk	0.60	0.90	0.98
Root	0.20	0.05	0.01

265

#### 266 **2.2.2.2 Dormancy**

267

268 In SEIB-DGVM, **deciduous PFTs** have dormant and growth phases. When the PFTs enter the bud  
269 flush phase, the NSC will be consumed. The NSC is allocated at the rates shown in Table 2.

270

#### 271 **2.2.2.3 Turnover**

272

273 Part of the NSC pools of leaves and roots is transformed into litter at the same fractional rates as  
274 in the turnover of general carbon pools for leaves and roots. This turnover is calculated at daily  
275 steps, regardless of the phenology phase.

276

#### 277 **2.2.2.4 Establishment**

278

279 The establishment process is performed on the last day of each simulation year in the SEIB-  
280 DGVM. The characteristics of the PFT are determined by five bioclimatic parameters: (1) the  
281 maximum temperature in the coldest month; (2) the maximum growing-degree day; (3) the  
282 minimum growing-degree day; (4) the minimum photosynthetically active radiation; and (5) the  
283 duration of drought. All new trees, independent of their PFT, start with a sapwood diameter of  
284 0.01 m and heartwood diameter of 0.00 m. Initially, these new trees have no leaves or fine roots.  
285 Their carbon cycle is therefore maintained by initial values of 250 g dry matter (DM) of  
286 assimilated carbon and 250 g DM of NSC ( $NSC_{leaf} = 10$  g,  $NSC_{trunk} = 190$  g, and  $NSC_{root} = 50$  g)  
287 from the litter pool.

288

### 289 **2.3 Validation of NSC for local and global simulations**

290

291 Observational NSC data for model validation were derived from Martínez-Vilalta et al. (2016),  
292 who reviewed 296 papers and summarized NSC dynamics in forests. Their data include total  
293 NSCs in leaves, trunks, and roots of mature terrestrial plants from observations lasting at least  
294 four months. These data were used for both the local-scale and the global-scale model validations  
295 mixed with other sources described below.

296

#### 297 **2.3.1 Validation at field points**

298



### 299 **2.3.1.1 Site descriptions**

300

301 For the **point-scale** validation, we selected locations where NSC data were available for all organs.  
302 **Four countries satisfied these criteria** and were used to validate the simulated NSC content in the  
303 plant organs: **Canada (boreal)**, Austria and Switzerland (temperate), and Panama (tropical). **At**  
304 **each site, the seasonality of the NSC was measured for at least four months**. We used local climate  
305 data from meteorological stations gap-filled by corrected gridded climate reanalysis data as the  
306 input at these sites. We ran the NSC module including the SEIB-DGVM with the location and  
307 climate provided and compared the model output with the observation data.

308 The boreal site **was** located near Alder Flats, Alberta, Canada (52°58'N, 114°59'W) in 2000.  
309 The site was dominated by boreal winter deciduous plants such as *Populus tremuloides*  
310 (Landhäuser and Lieffers, 2003). One of the temperate sites was located in the timberline ecotone  
311 at Mt. Patscherkofel to the south of Innsbruck, Austria (47°13'N, 11°27'E) in 2008 (Gruber et al.,  
312 2011). Temperate conifer species such as *Pinus cembra* were the dominating tree species. The  
313 mean annual air temperature is 2.5°C, with a maximum of 26.0°C in summer and a minimum of  
314 -28.0°C in winter. The mean annual precipitation is 995 mm. The other temperate site was at the  
315 Mont Noble, Canton Valais, Swiss Central Alps (46°12'N, 7°30'E) and was dominated by  
316 temperate conifers (*P. cembra* L.; Hoch et al., 2003) in 2000. The mean annual precipitation is  
317 630 mm. The growing season lasts from early May to early October, and the mean temperature  
318 during that time is 6.5°C. The tropical site was located at the Parque Natural Metropolitano near  
319 Panama City, the Republic of Panama in 1996 (85°8'N, 79°34'W; Würth et al., 2005). The site  
320 has mixed cover with 17 dominant species, including *Cecropia longipes* and *Anacardium*  
321 *excelsum*. The mean annual temperature is 27°C, and the mean annual precipitation was 2,120  
322 mm during 1993–1995 measured at 1.6 km from the site with a canopy crane (data from the  
323 Panama Canal Commission, meteorological and hydrological branch).

324

### 325 **2.3.1.2 Input climate data**

326

327 The SEIB-DGVM requires ten climatic variables as environmental drivers: air temperature, soil  
328 temperature at a depth of 50 cm (soil layer 1), soil temperature at a depth of 100 cm (soil layer  
329 2), soil temperature at a depth of 150 cm (soil layer 3), precipitation, shortwave radiation,  
330 longwave radiation, wind velocity, specific humidity, and diurnal range of air temperature. The  
331 input climate data were prepared by harmonizing a global reanalysis gridded climate dataset, the  
332 WATCH Forcing Data ERA-Interim (WFDEI, 0.5 × 0.5 degrees, 1979–2016,  
333 Weedon et al., 2018), and the climate generated by the SEIB generator (Tei et al., 2017), which  
334 is the monthly observation-based climatic datasets produced by Climatic Research Unit (CRU



335 TS4.00,  $0.5 \times 0.5$  degrees, 1901-2015, Harris et al., 2014) supplemented with the National  
336 Centers for Environmental Prediction/National Center for Atmospheric Research  
337 (NCEP/NCAR) daily climate datasets (Kalnay et al., 1996) for 1950, with local climatology  
338 recorded at meteorological stations near the sites. Local climatology in Panama is measured at  
339 the Parque Natural Metropolitano Canopy Crane meteorological station (1995–2019). The  
340 climatology in Austria (1979–2008) and Switzerland (1979–2000) was derived from the closest  
341 meteorological station to the field site under the European Climate Assessment (Klein et al.,  
342 2002, <https://www.ecad.eu>). WFDEI data were used for the climatology in Canada, except for  
343 precipitation data, which are measured in the Meteorological Service of Canada (1979–1984,  
344 [https://climate.weather.gc.ca/historical\\_data/search\\_historic\\_data\\_e.html](https://climate.weather.gc.ca/historical_data/search_historic_data_e.html)).

345 The reanalysis of daily WFDEI and SEIB climate data included daily records, which were  
346 corrected by regression models to local climate data. For temperature, humidity, and shortwave  
347 radiation values, local climatology were used directly and the daily WFDEI data supplemented  
348 by simple linear regression. Precipitation data and wind speeds were first adjusted to monthly and  
349 then annual averages and then scaled as a correction. WFDEI precipitation data were scaled after  
350 adjusting to the annual climatological precipitation of 995 mm in 2008 for Austria and 630 mm  
351 in 2000 for Switzerland. Longwave radiation was calculated using harmonized temperatures and  
352 humidities above (Brutsaert, 1975). Missing values were estimated via linear interpolation.  
353 Because soil temperature data were unavailable for local sites and for WFDEI, soil layer  
354 temperatures were calculated using the SEIB generator by regressing soil layer 1 on atmospheric  
355 temperature, soil layer 2 on layer 1, and layer 3 on layer 2. In Austria, humidity data were available  
356 from 2005. The WFDEI data were therefore used to estimate missing data via linear interpolation.  
357 In Canada, no observational data were available, except for temperature and precipitation.  
358 Precipitation in Canada was scaled with WFDEI data after adjusting to the total climatological  
359 precipitation for 1979–1984, shortwave radiation was taken from the WFDEI, and humidity data  
360 were harmonized in the same way as the humidity data in Austria.

361

### 362 **2.3.1.3 Simulation scheme**

363

364 To reach equilibrium conditions of the biomes, plant, and soil carbon pools, a 1000-year spin-up  
365 simulation was performed by looping the climate data and atmospheric CO<sub>2</sub> concentrations  
366 between 1979–2000. Building on the final conditions of the spin-up simulations, continuous  
367 simulations corresponding to 1979–2001 in Canada, 1979–2008 in Austria, 1979–2000 in  
368 Switzerland, and 1979–1995 in Panama were carried out, and the NSC dynamics were compared  
369 with field data.

370



### 371 2.3.2 Validation at a global scale

372

373 In the global-scale simulation, the NSC seasonality in the SEIB-DGVM was validated using  
374 CRU/NCEP/MIROC integrated data ( $0.5 \times 0.5$  degrees, 1850-2100, Tei et al., 2017, Watanabe et  
375 al., 2011) as climatic input. SEIB-DGVM-NSC ver 1.0 is expected to simulate on future scenarios,  
376 thus the different climate data that cover longer period than that of section 2.3.1.2. are used for  
377 validation at a global scale. The SEIB-DGVM categorizes plant species into 16 PFTs for global-  
378 scale simulations.

379 For the validation, we used all available NSC data from the given climate zone. The outputs  
380 of the SEIB-DGVM include two boreal biome types (evergreen and deciduous forests), three  
381 temperate biome types (conifer, broad-leaved evergreen, and deciduous forests), and two tropical  
382 biome types (evergreen and deciduous forests), whereas the observations included two boreal  
383 biome types (conifer and deciduous forests), three temperate biome types (conifer, evergreen, and  
384 deciduous forests), and two tropical biome types (evergreen and deciduous forests). The model  
385 outputs and observation data were compared for each climate zone. Global climate data were  
386 available from 1850 to 2005. The first 30 years (1850–1880) were therefore looped for a 1000-  
387 year spin-up simulation. After the spin-up, simulations were run for the period 1850–2005. The  
388 NSC dynamics from the period 1975–2005 were used for model validation.

389

### 390 2.4 Parameterization of NSC functions

391

392 Hoch et al. (2003) have reported that the  $NSC_{leaf}$  of temperate trees varies between 7%–20% of  
393 the total leaf DM. They determined the seasonal mean of the  $NSC_{trunk}$  in sapwood of temperate  
394 deciduous trees and temperate evergreen trees to be  $4.7\% \pm 0.1\%$  of DM and  $1.8\% \pm 0.1\%$  of DM,  
395 respectively. There were no significant seasonal differences. The mean  $NSC_{root}$  was less than 1.5%  
396 of the root DM throughout the whole season (Gruber et al., 2012), and the total NSC of temperate  
397 trees was around 4%–5% of the DM during the growing season (Gruber et al., 2011). For tropical  
398 trees, the  $NSC_{trunk}$  and  $NSC_{root}$  were 8%–10% of their biomass, whereas the  $NSC_{leaf}$  fluctuated  
399 within 5%–9% of leaf biomass (Würth et al., 2005). Landhäusser and Lieffers (2003) have  
400 reported that the  $NSC_{root}$  of boreal trees, which is used to support leaf flush and root growth, is  
401 3%–4% of their root mass. The stemwood  $NSC_{trunk}$  concentration is  $\sim 18 \text{ mg g}^{-1}$  of the DM  
402 (Carbone et al., 2013). Because of limited observational data, the parameters of the NSC processes  
403 were derived mostly from the values observed at each site used for point-scale validation, and the  
404 maximums of simulated NSCs were corrected so that they were in the range of measured NSCs.

405 First, the parameter  $b$  in Eq. (10) was determined from the percentage of NSC and the biomass  
406 in January. The parameter  $a$  was then adjusted so that the fluctuations of the NSCs did not exceed



407 the measured mean seasonal NSCs. The parameter  $a$  in Eq. (10) controls the minimum amount of  
 408 photosynthetically fixed carbon mobilized for the NSC pools. In temperate zones, the value of  $a$   
 409 differs before and after July, and the NSC peaks around mid-summer. In contrast, in tropical zones,  
 410 the amount of NSC in leaves and trunks decreases throughout the spring–summer.

411 Because the NSCs depend on the environmental conditions at the field sites, which could not  
 412 be incorporated into the global simulation, different parameters were used when validating point-  
 413 scale and global-scale results. Tables 3 and 4 show the parameters used for validation. Parameter  
 414 values unrelated to the NSC module remain at the default values of the SEIB-DGVM (Sato et al.,  
 415 2007).

416

417 **Table 3.** Parameters of NSC pool size function for point-scale simulation

Organ	Canada	Austria	Switzerland	Panama
Leaf	$a: 0.4 \times 10^{-3}, b: 0.09$	$a: 0.065 \times 10^{-3}, b:$ 0.04 (Jul–Oct)	$a: 0.1 \times 10^{-3}, b: 0.13$ (Jul–Oct)	$a: 0.06, b: -0.15 \times$ $10^{-3}$ (Jun–Nov)
		$a: 0.135 \times 10^{-3}, b:$ 0.04 (others)	$a: 0.8 \times 10^{-3}, b: 0.13$ (others)	$a: 0.06, b: 0.15 \times 10^{-3}$ (others)
Trunk	$a: 0.03 \times 10^{-3}, b: 0.06$	$a: 0.05 \times 10^{-3}, b: 0.02$	$a: 0.01 \times 10^{-3}, b:$ 0.02	$a: 0.1, b: -0.35 \times 10^{-3}$ (Jun–Nov)
Root	$a: 0.06 \times 10^{-3}, b: 0.14$	$a: 0.01 \times 10^{-3}, b: 0.02$	$a: 0.003 \times 10^{-3}, b:$ 0.06	$a: 0.1, b: 0$ (others)
				$a: 0.04, b: 0.005$

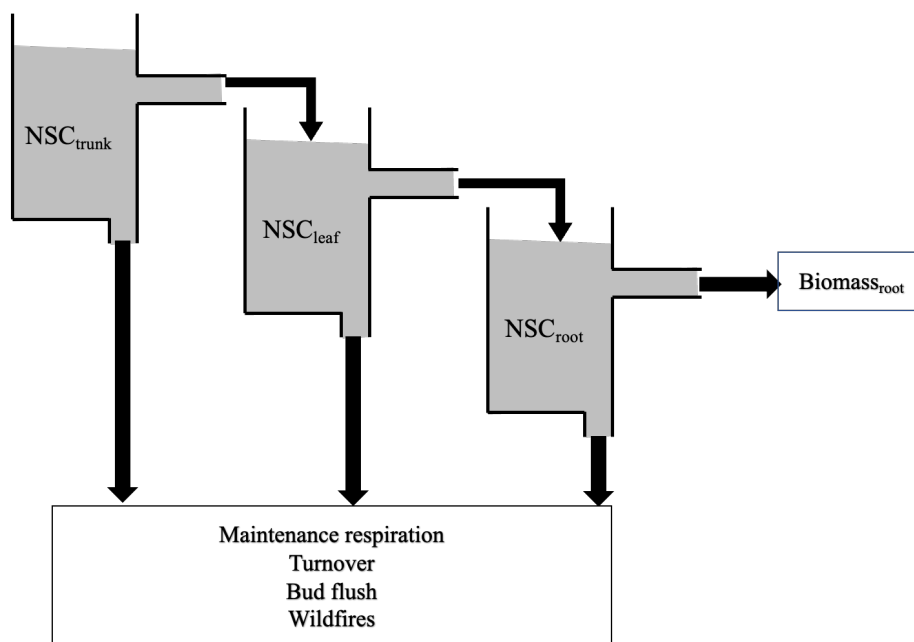
418

419

420 **Table 4.** Parameters of NSC pool size functions for global-scale simulation

Organ	Boreal	Temperate	Tropical
Leaf	$a: 0.4 \times 10^{-3}, b: 0.09$	$a: 0.1 \times 10^{-3}, b: 0.13$ (Jul–Oct)	$a: 0.06, b: -0.15 \times 10^{-3}$ (May– Jul)
		$a: 0.7 \times 10^{-3}, b: 0.13$ (others)	$a: 0.06, b: 0.15 \times 10^{-3}$ (others)
Trunk	$a: 0.03 \times 10^{-3}, b: 0.06$	$a: 0.01 \times 10^{-3}, b: 0.04$	$a: 0.1, b: -0.35 \times 10^{-3}$ (May– Jul)
Root	$a: 0.06 \times 10^{-3}, b: 0.14$	$a: 0.003 \times 10^{-3}, b: 0.06$	$a: 0.1, b: 0$ (others)
			$a: 0.06 \times 10^{-3}, b: 0.0145$

421



422

423 **Figure 1. Schematic model** structure of NSC pool.

424

425



## 426 **3 Results**

427

### 428 **3.1 Seasonality of NSC at the point scale**

429

#### 430 **3.1.1 Canada**

431

432 The fact that the dominant PFT in the simulations was boreal deciduous trees was consistent with  
433 observations at the site in Canada. The model simulated an increase in the NSC of leaves from 80  
434  $\text{mg g}^{-1}$  to 203  $\text{mg g}^{-1}$ , whereas the observed NSC values were 89  $\text{mg g}^{-1}$  in May and 185  $\text{mg g}^{-1}$   
435 in August (Fig. 2a). The modeled NSCs in leaves therefore captured the increasing trend during  
436 the growing season, but the simulations overestimated the maximum NSC a little. The observed  
437 NSCs in trunks fluctuated from 90  $\text{mg g}^{-1}$  to 192  $\text{mg g}^{-1}$  during a year with no specific seasonal  
438 trend (Fig. 2e). The model outputs in trunks were in the range 56–76  $\text{mg g}^{-1}$ . Although the  
439 observed fluctuations exceeded the modeled outputs, the modeled outputs were within one  
440 standard deviation of the observations. The range of the observed NSCs in roots was 97–138  $\text{mg g}^{-1}$   
441  $\text{g}^{-1}$ , whereas the range of the modeled NSCs was 117–132  $\text{mg g}^{-1}$  (Fig. 2i). However, the  
442 observations peaked in August 2001 and in October 2002. The modeled NSCs of roots differed  
443 from the observed NSCs because the former peaked during August in both years. Overall, the  
444 simulated NSCs agreed well with the observed data (Fig. 3; RMSE = 69.92  $\text{mg g}^{-1}$ ,  $r = 0.21$ ).

445

#### 446 **3.1.2 Austria**

447

448 The fact that the dominant PFT in the simulations was temperate conifer forests was consistent  
449 with observations at the site in Austria. The modeled NSCs in leaves accumulated until July with  
450 a maximum of 142  $\text{mg g}^{-1}$ . This pattern was similar to the observed seasonality of the NSCs,  
451 which peaked at 150  $\text{mg g}^{-1}$  (Fig. 2b). The modeled NSCs in trunks were stable in the range 19–  
452 26  $\text{mg g}^{-1}$ , and the observations were within the range 18–38  $\text{mg g}^{-1}$ , with no specific seasonality  
453 (Fig. 2f). The modeled values were interspersed between the observations. The modeled NSCs in  
454 roots varied in a curvilinear manner from 18 to 26  $\text{mg g}^{-1}$ , a range that was similar to the range of  
455 the observed NSCs, 13–32  $\text{mg g}^{-1}$  (Fig. 2j). The seasonality and magnitudes of the modeled NSCs  
456 were consistent with observations (Fig. 3; RMSE = 9.52  $\text{mg g}^{-1}$ ,  $r = 0.95$ ).

457

#### 458 **3.1.3 Switzerland**

459

460 The dominant PFT in the simulations corresponded to the temperate conifers observed at the field  
461 site. The NSCs in the tree leaves accumulated during early spring and reached up to 222  $\text{mg g}^{-1}$



462 (Fig. 2c). The decrease of the NSCs after July to a minimum of  $135 \text{ mg g}^{-1}$  was similar to the  
463 decline of the observed NSCs to a minimum of  $124 \text{ mg g}^{-1}$ . The modeled NSCs in trunks fell in  
464 the range  $13\text{--}16 \text{ mg g}^{-1}$ , which was overlapped with the range of the observed NSCs in trunks,  
465  $15\text{--}33 \text{ mg g}^{-1}$  (Fig. 2g), and the modeled NSCs all fell within one standard deviation of the  
466 observations. The modeled NSCs in roots increased gradually from  $45$  to  $62 \text{ mg g}^{-1}$ , which is  
467 similar to the observed range of observations,  $48\text{--}64 \text{ mg g}^{-1}$  (Fig. 2k). The simulations captured  
468 the amounts and seasonal patterns of the NSCs in the different organs and produced results that  
469 compared well with observations (Fig. 3;  $\text{RMSE} = 25.83 \text{ mg g}^{-1}$ ,  $r = 0.91$ ).

470

#### 471 **3.1.4 Panama**

472

473 While a wide range of woody species was found at the Panama site, in the simulation the tropical  
474 evergreen PFT became dominant. The simulations showed that the NSCs in leaves were stored  
475 during winter and were then gradually consumed from July to October, when they reached a  
476 minimum of  $52 \text{ mg g}^{-1}$  (Fig. 2d). The observed NSCs in leaves likewise decreased from  $69$  to  $48$   
477  $\text{mg g}^{-1}$  between August and October. The model therefore followed the observed seasonality of  
478 the leaf NSCs. The modeled NSCs in trunks fell in the range  $35\text{--}73 \text{ mg g}^{-1}$  (Fig. 2h). The slight  
479 decrease of the modeled NSCs in trunks during the summer was not apparent in the observations.  
480 However, the simulated values fell within the range of the observed NSCs,  $27\text{--}97 \text{ mg g}^{-1}$ . The  
481 simulated NSCs in roots fell in the range  $23\text{--}55 \text{ mg g}^{-1}$ ; the observed NSCs ranged from  $43$  to  $70$   
482  $\text{mg g}^{-1}$  (Fig. 2l). Despite the weak correlation between simulated and observed NSCs, the model  
483 results were within the acceptable margin of error (Fig. 3;  $\text{RMSE} = 20.75 \text{ mg g}^{-1}$ ,  $r = 0.08$ ).

484

#### 485 **3.2 Seasonality at a global scale**

486

487 For validation at a global scale, the mean annual NSCs from the model were compared with the  
488 observed mean annual NSCs in boreal, temperate, and tropical regions (Table 5). The model  
489 simulated the amounts of NSCs in forest tree trunks in all climate regions with high accuracy. The  
490 modeled NSCs in the trunks of trees in boreal forests averaged  $47.48 \pm 18.35 \text{ mg g}^{-1}$ , which  
491 compared favorably with the observed average of  $76.67 \pm 23.68 \text{ mg g}^{-1}$ . In temperate forests, the  
492 modeled NSCs of trunks averaged  $44.78 \pm 6.82 \text{ mg g}^{-1}$ , which was close to the observed average of  
493  $51.59 \pm 22.63 \text{ mg g}^{-1}$ . The modeled NSCs of trunks in tropical forests averaged  $66.68 \pm 18.79 \text{ mg g}^{-1}$ ,  
494 which was close to the average of the observations,  $106.23 \pm 32.52 \text{ mg g}^{-1}$ . Although the modeled  
495 NSCs in leaves of temperate and tropical forests were close to observed values, the modeled NSCs  
496 in leaves of boreal forests underestimated the observed values. Moreover, the modeled NSCs in  
497 roots of tropical forests were smaller than the observed NSCs. Overall, the simulated NSCs of all





498 organs of forest trees in all climate regions agreed reasonably well with observations (Fig. 4;  
 499 RMSE = 66.75 mg g<sup>-1</sup>,  $r = 0.17$ ). The model could simulate the NSCs with high accuracy, with  
 500 the exception of the NSCs of tree leaves in boreal forests and of tree roots in tropical forests (Fig.  
 501 4; RMSE = 34.15 mg g<sup>-1</sup>,  $r = 0.71$ ).

502  
 503 **Table 5.** Comparison of modelled and observed annual mean NSC concentrations (mg g<sup>-1</sup>) on a  
 504 global scale. The observed results are represented as the mean ± 1 standard deviation

	Boreal		Temperate		Tropical	
	Observation	Model	Observation	Model	Observation	Model
Leaf	202.80 ± 19.97	94.91 ± 42.91	127.10 ± 25.6	170.90 ± 46.54	86.42 ± 20.21	46.92 ± 16.20
Trunk	76.67 ± 23.68	47.48 ± 18.35	51.59 ± 22.63	44.78 ± 6.82	106.23 ± 32.52	66.68 ± 18.79
Root	118.49 ± 13.24	105.80 ± 40.82	67.65 ± 18.79	23.58 ± 10.57	170.40 ± 36.49	44.55 ± 15.15

505

### 506 3.3 Woody biomass and total NSCs on a global scale

507

508 The average of the total GPP simulated from the new model during 1976–2005 was 123 PgC  
 509 year<sup>-1</sup>. The model estimated the mean total woody biomass to be 282 PgC year<sup>-1</sup> in boreal zones,  
 510 100 PgC year<sup>-1</sup> in temperate zones, and 337 PgC year<sup>-1</sup> in tropical zones globally during 1976–  
 511 2005. In boreal zones such as North America and Russia, the mean concentration of total NSCs  
 512 was 4.98% ± 1.87% of total woody biomass (Fig. 5). In temperate zones such as Asia, the mean  
 513 concentration of total NSCs was 4.67% ± 0.54% of total woody biomass. Total NSCs of tropical  
 514 forests in South America and Africa were 6.19% ± 1.66% of their total woody biomass. Mean  
 515 values of the simulated total NSCs relative to total woody biomass were close to previous  
 516 estimates for temperate and tropical forests (Table 6). The total NSCs of temperate, broad-leaved,  
 517 evergreen forests were 4.63% ± 0.50% of the corresponding woody biomass reported by Smith et al.  
 518 (2018). The total NSCs of temperate conifer forests were 4.72% ± 0.58% of total woody biomass,  
 519 which was close to the figure of 4% reported by Körner (2003). According to Würth et al. (2005),  
 520 the percentages of woody biomass contributed by NSCs are 4%–8% in tropical forests, 4.66% ±  
 521 1.28% in tropical deciduous forests, and 7.11% ± 1.08% in tropical evergreen forests. These  
 522 observed percentages are close to our simulated values.

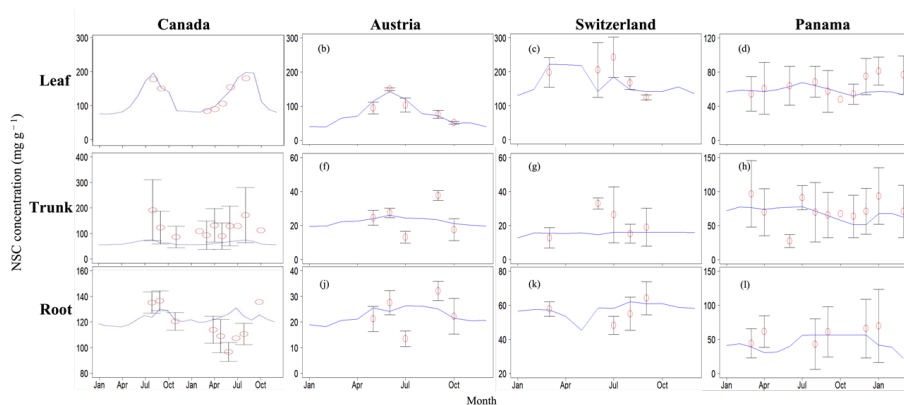
523

524 **Table 6.** Comparison of modeled mean NSC concentrations to observed total NSC concentrations (%)  
 525 for different types of biomes. The simulated results are expressed as the mean ± 1 standard deviation



	Total NSC	Leaf	Trunk	Root	Observation
Boreal deciduous	3.41 ± 1.58	0.05 ± 0.09	3.06 ± 1.23	0.30 ± 0.62	
Boreal evergreen	6.06 ± 1.16	0.75 ± 0.38	4.73 ± 1.29	0.58 ± 0.37	
Temperate deciduous	2.30 ± 0.33	0.02 ± 0.01	2.25 ± 0.31	0.03 ± 0.01	1.0–12.5 (Gough et al., 2009)
Temperate broad-leaved evergreen	4.63 ± 0.50	0.49 ± 0.20	4.10 ± 0.56	0.04 ± 0.03	2.6–4.4 (Smith et al., 2018)
Temperate conifer	4.72 ± 0.58	0.89 ± 0.38	3.77 ± 0.73	0.08 ± 0.04	4.0 (Körner, 2003)
Tropical deciduous	4.66 ± 1.28	0.04 ± 0.03	4.60 ± 1.27	0.03 ± 0.02	4.0–8.0 (Würth et al., 2005)
Tropical evergreen	7.11 ± 1.08	0.08 ± 0.03	7.00 ± 1.08	0.02 ± 0.01	4.0–8.0 (Würth et al., 2005)

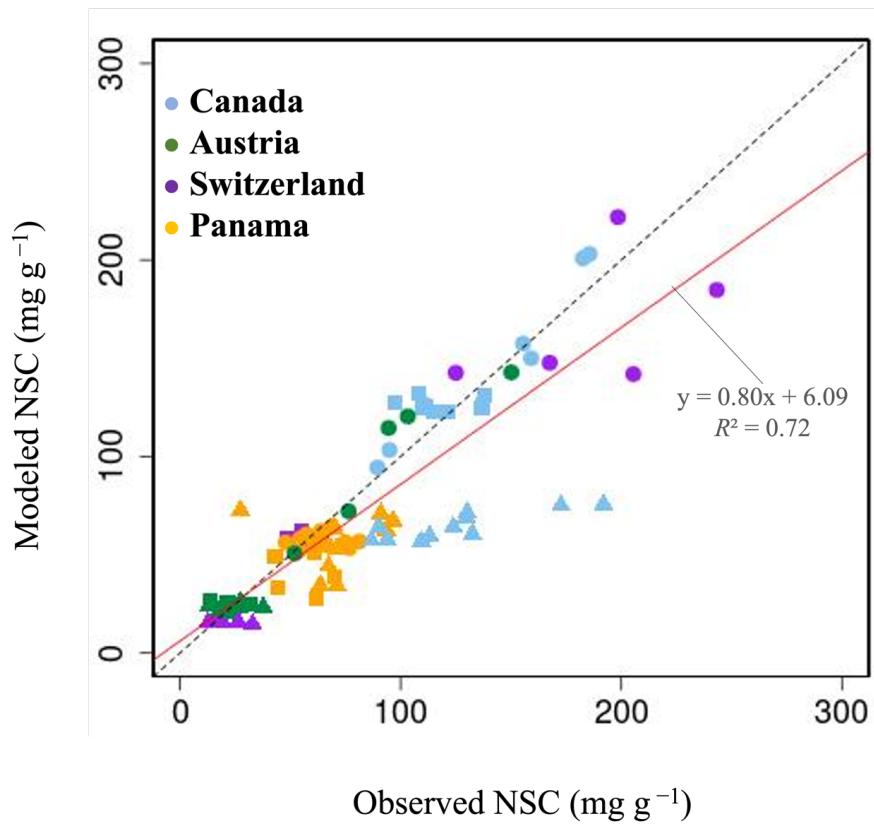
526



527

528 **Figure 2.** Validation of the modeled NSC with observed NSC data ( $\text{mg g}^{-1}$ ) at sites in Canada,  
 529 Austria, Switzerland, and Panama. Red circles indicate the observed data, and blue lines indicate  
 530 the modeled NSC. The observed results are represented as mean  $\pm$  1 standard deviation.

531

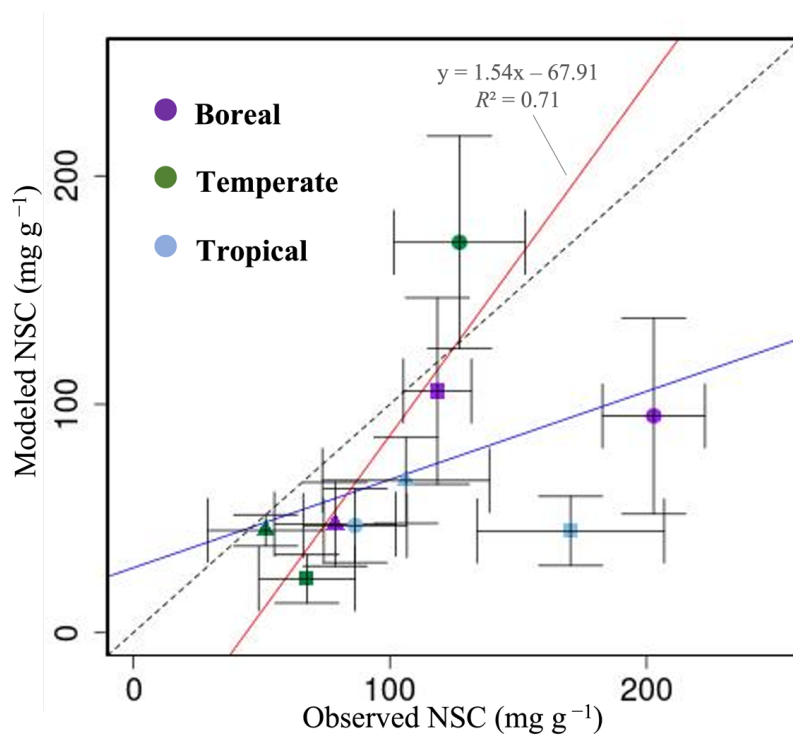


532

533 **Figure 3.** Plot of modeled NSC ( $\text{mg g}^{-1}$ ) with observed NSC ( $\text{mg g}^{-1}$ ) at a point scale. ●, leaves;

534 ▲, trunks; ■, roots. For all data,  $r$  is 0.72, and RMSE is  $29.65 \text{ mg g}^{-1}$ .

535

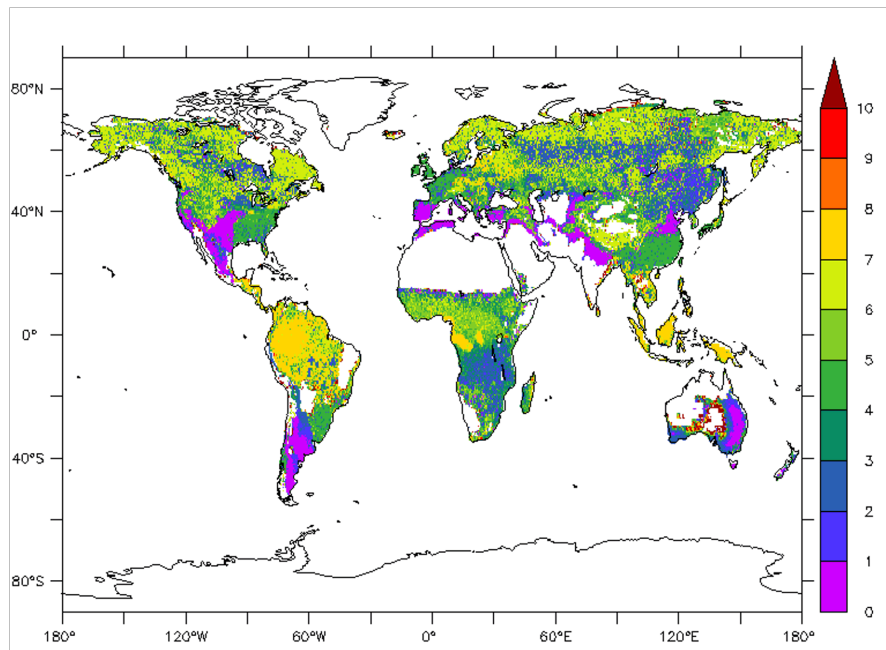


536

537 **Figure 4.** Plot of modeled NSC (mg g<sup>-1</sup>) with observed NSC (mg g<sup>-1</sup>) at a global scale. ●, leaves;

538 ▲, trunks; ■, roots.

539



540

541 **Figure 5. Mean total NSC concentration relative to total woody biomass during 1976–2005 (%).**

542

543



544 **4 Discussion**

545

546 **On a point scale**, the modeled NSCs for boreal forests in Canada were close to the observed  
547 NSCs. The seasonality of the modeled NSCs in leaves was consistent with observations.  
548 However, the seasonality of NSC in roots differed from the observations because there were  
549 insufficient observations in boreal regions that enabled assessment of the seasonality of NSCs in  
550 all organs. The seasonality of NSCs in roots is therefore still unclear. In temperate zones, the  
551 model simulated the observed NSCs very accurately. The simulated NSCs of temperate forests  
552 were close to observed values in Austria and Switzerland. The simulations showed that the  
553 NSCs in leaves were consumed in winter for bud flush, and the leaves accumulated NSCs  
554 during the growing season. This pattern corresponded to the seasonality reported in Asaadi et al.  
555 (2018) and Furze et al. (2019). In the tropical zones, the model also captured a seasonality of  
556 NSCs that was similar to observations. The NSC concentration in the canopy of tropical forests  
557 decreased from June to August to satisfy increased maintenance demands (Signori-Müller et al.,  
558 2022; Würth et al., 2005). The simulated NSCs in leaves followed a similar pattern from June to  
559 August, and the simulated NSCs in leaves, trunks, and roots were close to observed values.

560 **On** a global scale, the simulated NSC values of all climate regions agreed with the observed  
561 data, except for the leaves of boreal forests and roots of tropical forests. The new function,  
562 which was validated at the point scale, could therefore perform well on a global scale. The  
563 NSCs in trunks, which contain the greatest amounts of carbon in trees, were simulated  
564 accurately in all climate regions. The new function could therefore calculate the total NSC  
565 storage in trees with great accuracy.

566 The model with the new function calculated the global GPP to be  $123 \text{ PgC year}^{-1}$ , which is  
567 close to the previous estimates of  $106.2 \pm 2.9 \text{ PgC year}^{-1}$  by Zheng et al. (2020) and  $130 \pm 1.6$   
568  $\text{PgC year}^{-1}$  by Madani et al. (2020). Moreover, the simulated mean total woody biomass for  
569 boreal forests was  $282 \text{ PgC year}^{-1}$ , which is within the range of  $249\text{--}295 \text{ PgC year}^{-1}$  reported by  
570 Pan et al. (2011). The simulated woody biomass of  $100 \text{ PgC year}^{-1}$  for temperate forests was  
571 within the observed range of  $59\text{--}139 \text{ PgC year}^{-1}$  (Hui et al., 2020) and a little lower than the  
572 range of  $113\text{--}125 \text{ PgC year}^{-1}$  for other temperate forests (Pan et al., 2011). The calculated total  
573 woody biomass of  $337 \text{ PgC year}^{-1}$  for tropical forests was within the range of  $212\text{--}340 \text{ PgC}$   
574  $\text{year}^{-1}$  reported by Hui et al. (2020) and was not very different from the estimates of  $378\text{--}564$   
575  $\text{PgC year}^{-1}$  by Pan et al. (2011), and  $200\text{--}300 \text{ PgC year}^{-1}$  by Mitchard (2018). Furthermore, the  
576 total NSCs relative to total biomass output from the new function for temperate and tropical  
577 biome types agreed with previous research. The total NSC of boreal biome types could not be  
578 compared with observations due to lack of data.

579 The new model **has a high potential to simulate various biotic effects on terrestrial ecosystems**



580 more accurately by calculating the NSC dynamics within each plant organ. The NSCs stored in  
581 the trunk and roots compensate for the deficit of CO<sub>2</sub> uptake in trees under stress, and the NSC  
582 stored in roots is potentially indispensable for tree recovery after disturbances (Herrera-Ramírez  
583 et al., 2020). Furthermore, the NSC changes in the trunk and roots are better indicators of carbon  
584 source–sink relationships under elevated CO<sub>2</sub> conditions than the NSC changes in leaves because  
585 the **NSC concentrations in leaves** increase under elevated CO<sub>2</sub> conditions irrespective of growth  
586 conditions. The NSC changes in the trunk and roots are therefore more tied to the carbon balance  
587 of plant bodies (Körner, 2003). Simulation of the dynamics of NSC in the three compartments in  
588 this research contributes to understanding plant growth and the response of carbon dynamics in  
589 each organ to increasing atmospheric CO<sub>2</sub>.

590 Carbon starvation **may also be the main cause of plant death during drought** when  
591 photosynthesis decreases and water stress increases (McDowell et al., 2008). If reduced  
592 photosynthetic rates cannot supply enough carbon for NSC accumulation during drought, there  
593 will be greater canopy dieback in the next season. Plants therefore prioritize NSC storage, even  
594 when no excess carbon is available (Hartmann et al., 2020). At times, plants are unable to allocate  
595 carbon for this NSC defense mechanism, and their reduced ability to recover from biotic attacks  
596 such as defoliation caused by insect pests leads to decreased growth rates, less restoration of NSC,  
597 and lower survival rates. These processes may culminate in broad-scale tree **mortalities**  
598 (McDowell, 2011; Chen et al., 2017).

599 The new model introduced NSC compartments in leaves, trunk, and roots that were validated  
600 at the point and global scales. Use of the model developed here enabled simulation of the  
601 environmental effects on forests resulting from the changing amount of NSC in each organ. The  
602 simulations **depicted the NSC changes in the trunk especially well**. The model could thus be used  
603 as an indicator of the carbon cycle in terrestrial ecosystems to understand the effect of climate  
604 change. Simulation of photosynthetic carbon allocated into NSC storage in leaves, trunks, and  
605 roots enables a more dynamic simulation of the carbon cycle between terrestrial ecosystems and  
606 the atmosphere.

607 However, there were still some limitations to this research. We considered two potential  
608 limitations that could lead to some discrepancies between the modeled and measured NSC values.  
609 First, the relatively coarse spatial resolution of 0.5°×0.5° gridded climate data at the global scale  
610 could not depict the details of local climates derived from observations. These differences were  
611 especially important in the case of precipitation and soil properties, which play a key role in NSC  
612 dynamics. Lowering of the water level in soils causes damage to the hydraulic conductivity of the  
613 phloem tube, which leads to a **decline of phloem conductance** at the stem level (Dannoura et al.,  
614 2018; Sevanto, 2014). This cessation of phloem transport could change the allocation of  
615 photosynthetic products to plant growth and affect the ability of the trees to accumulate NSCs



616 (Dannoura et al., 2018).  
617 Second, the scarcity of ground-measured NSC seasonality prevented us from having more average  
618 information on NSC concentrations, especially in the tropical and boreal regions, where there  
619 were fewer available data. The NSC seasonality differs between biome types, but because it is  
620 difficult to measure NSC dynamics, there is a lack of long-term data for each biome type. Hence,  
621 parameters were tuned to simulate the same seasonality for all the biome types in a given climate  
622 zone in our study. The fact that the NSC allocation was further influenced by environmental  
623 conditions caused the allocation patterns to change within the same biome type. The NSC  
624 allocation to roots was favored over aboveground allocations when soil resources were lacking,  
625 and tree size was considered an important determinant of carbon allocation as well as aridity  
626 (Hartmann et al., 2020). Because we pooled data for each organ from different measurement sites  
627 for global-scale validation, environmental effects on the data could not be measured. In addition  
628 to the above factors, the number of samples and duration of observations differed between the  
629 various studies. These differences led to no explicit NSC seasonality. These potential sources of  
630 error in the field measurements jeopardized the model performances.

631

## 632 **5 Conclusions**

633

634 In this study, a new NSC model was incorporated into the SEIB-DGVM to understand the effect  
635 of NSC allocation on global forest dynamics through competition and establishment among  
636 individual trees. The new module calculated the NSC dynamics of three organs—leaves, trunk,  
637 and roots—and the general NSC seasonality based on ground measurements was determined for  
638 biome types in three climate zones: boreal, temperate, and tropical. The NSC seasonality was  
639 validated at four sites: Canada (boreal), Austria and Switzerland (temperate), and Panama  
640 (tropical). The mean values of simulated NSC concentration agreed reasonably well with  
641 observed data on a global scale.

642 The model enabled us to simulate the biotic effects resulting from insufficient NSC caused  
643 by factors such as carbon starvation and insect pests that are otherwise difficult to measure in  
644 terrestrial ecosystems globally. The difference of the NSC dynamics in the organs under  
645 elevated CO<sub>2</sub> conditions highlighted the importance of modeling the organs separately when  
646 studying environmental stresses. As more observation data about NSC dynamics become  
647 available, the model can be further improved and can contribute to the simulations of the  
648 passive biome shifts that may occur globally.

649

### 650 *Code and data availability*

651 The model code used in this study is archived at <https://doi.org/10.5281/zenodo.7021459>.





652

653 *Author contributions.* T.K. conceived and supervised this study and acquired the funding. H.N.  
654 developed the model code and carried out the analysis and produced the figures. H.N. prepared  
655 the original draft, and T.K., and L.V. reviewed it. L.W. prepared the modeling environment. All  
656 authors have read and agreed to the published version of the manuscript.

657

658 *Competing interests.* The authors declare that they have no conflicts of interest.

659

660 *Acknowledgments.* This study was funded by the Nippon Life Insurance Company. This work  
661 was supported by JSPS KAKENHI Grant Number JP 22J20286.

662 We thank all the contributors. Dr. Epron and Dr. Dannoura in Kyoto University provided  
663 assistance. Dr. Hajima and Dr. Mori converted MIROC and CRU/NCEP climate data for  
664 CRU/NCEP/MIROC integrated data. We acknowledge the data provided by the European Climate  
665 Assessment & Dataset project.

666

## 667 **References**

668

669 Adams, H. D., Germino, M. J., Breshears, D. D., Barron-Gafford, G. A., Guardiola-Claramonte,  
670 M., Zou, C. B. and Huxman, T. E.: Nonstructural leaf carbohydrate dynamics of *Pinus edulis*  
671 during drought-induced tree mortality reveal role for carbon metabolism in mortality  
672 mechanism, *New Phytol.*, 197(4), 1142–1151, doi:10.1111/nph.12102, 2013.

673

674 Adams, H. D., Zeppel, M. J. B., Anderegg, W. R. L., Hartmann, H., Landhäusser, S. M., Tissue,  
675 D. T., Huxman, T. E., Hudson, P. J., Franz, T. E., Allen, C. D., Anderegg, L. D. L., Barron-  
676 Gafford, G. A., Beerling, D. J., Breshears, D. D., Brodribb, T. J., Bugmann, H., Cobb, R. C.,  
677 Collins, A. D., Dickman, L. T., Duan, H., Ewers, B. E., Galiano, L., Galvez, D. A., Garcia-  
678 Forner, N., Gaylord, M. L., Germino, M. J., Gessler, A., Hacke, U. G., Hakamada, R., Hector,  
679 A., Jenkins, M. W., Kane, J. M., Kolb, T. E., Law, D. J., Lewis, J. D., Limousin, J. M., Love,  
680 D. M., Macalady, A. K., Martínez-Vilalta, J., Mencuccini, M., Mitchell, P. J., Muss, J. D.,  
681 O'Brien, M. J., O'Grady, A. P., Pangle, R. E., Pinkard, E. A., Piper, F. I., Plaut, J. A., Pockman,  
682 W. T., Quirk, J., Reinhardt, K., Ripullone, F., Ryan, M. G., Sala, A., Sevanto, S., Sperry, J. S.,  
683 Vargas, R., Vennetier, M., Way, D. A., Xu, C., Ypez, E. A. and McDowell, N. G.: A multi-  
684 species synthesis of physiological mechanisms in drought-induced tree mortality, *Nat. Ecol.*  
685 *Evol.*, 1(9), 1285–1291, doi:10.1038/s41559-017-0248-x, 2017.

686

687 Asaadi, A., Arora, V. K., Melton, J. R. and Bartlett, P.: An improved parameterization of leaf area



- 688 index (LAI) seasonality in the Canadian Land Surface Scheme (CLASS) and Canadian  
689 Terrestrial Ecosystem Model (CTEM) modelling framework, *Biogeosciences*, 15(22), 6885–  
690 6907, doi:10.5194/bg-15-6885-2018, 2018.
- 691
- 692 Braakhekke, M. C., Doelman, J. C., Baas, P., Müller, C., Schaphoff, S., Stehfest, E. and Van  
693 Vuuren, D. P.: Modeling forest plantations for carbon uptake with the LPJmL dynamic global  
694 vegetation model, *Earth Syst. Dyn.*, 10(4), 617–630, doi:10.5194/esd-10-617-2019, 2019.
- 695
- 696 Brutsaert, W.: On a derivable formula for long - wave radiation from clear skies, *Water Resour.*  
697 *Res.*, 11(5), 742-744, doi:10.1029/WR011i005p00742, 1975.
- 698
- 699 Carbone, M. S., Czimczik, C. I., Keenan, T. F., Murakami, P. F., Pederson, N., Schaberg, P. G.,  
700 Xu, X. and Richardson, A. D.: Age, allocation and availability of nonstructural carbon in  
701 mature red maple trees, *New Phytol.*, 200(4), 1145–1155, doi:10.1111/nph.12448, 2013.
- 702
- 703 Chen, Z., Wang, L., Dai, Y., Wan, X. and Liu, S.: Phenology-dependent variation in the non-  
704 structural carbohydrates of broadleaf evergreen species plays an important role in determining  
705 tolerance to defoliation (or herbivory), *Sci. Rep.*, 7(1), 1–11, doi:10.1038/s41598-017-09757-  
706 2, 2017.
- 707
- 708 Chuste, P. A., Maillard, P., Bréda, N., Levillain, J., Thirion, E., Wortemann, R. and Massonnet,  
709 C.: Sacrificing growth and maintaining a dynamic carbohydrate storage are key processes for  
710 promoting beech survival under prolonged drought conditions, *Trees - Struct. Funct.*, 34(2),  
711 381–394, doi:10.1007/s00468-019-01923-5, 2020.
- 712
- 713 Dannoura, M., Epron, D., Desalme, D., Massonnet, C., Tsuji, S., Plain, C., Priault, P. and Gérant,  
714 D.: The impact of prolonged drought on phloem anatomy and phloem transport in young  
715 beech trees, *Tree Physiol.*, 39(2), 201–210, doi:10.1093/treephys/tpy070, 2018.
- 716
- 717 Dietze, M. C., Sala, A., Carbone, M. S., Czimczik, C. I., Mantoosh, J. A., Richardson, A. D. and  
718 Vargas, R.: Nonstructural carbon in woody plants, *Annu. Rev. Plant Biol.*, 65(June 2014),  
719 667–687, doi:10.1146/annurev-arplant-050213-040054, 2014.
- 720
- 721 Furze, M. E., Huggett, B. A., Aubrecht, D. M., Stolz, C. D., Carbone, M. S. and Richardson, A.  
722 D.: Whole-tree nonstructural carbohydrate storage and seasonal dynamics in five temperate  
723 species, *New Phytol.*, 221(3), 1466–1477, doi:10.1111/nph.15462, 2019.



- 724  
725 Gough, C. M., Flower, C. E., Vogel, C. S. and Curtis, P. S.: Phenological and temperature controls  
726 on the temporal non-structural carbohydrate dynamics of *Populus grandidentata* and *Quercus*  
727 *rubra*, *Forests*, 1(1), 65–81, doi:10.3390/f1010065, 2010.
- 728  
729 Gough, C. M., Flower, C. E., Vogel, C. S., Dragoni, D. and Curtis, P. S.: Whole-ecosystem labile  
730 carbon production in a north temperate deciduous forest, *Agric. For. Meteorol.*, 149(9), 1531–  
731 1540, doi:10.1016/j.agrformet.2009.04.006, 2009.
- 732  
733 Gruber, A., Pirkebner, D., Oberhuber, W. and Wieser, G.: Spatial and seasonal variations in mobile  
734 carbohydrates in *Pinus cembra* in the timberline ecotone of the Central Austrian Alps, *Eur. J.*  
735 *For. Res.*, 130(2), 173–179, doi:10.1007/s10342-010-0419-7, 2011.
- 736  
737 Gruber, A., Pirkebner, D., Florian, C. and Oberhuber, W.: No evidence for depletion of  
738 carbohydrate pools in Scots pine (*Pinus sylvestris* L.) under drought stress, *Plant Biol.*, 14(1),  
739 142–148, doi:10.1111/j.1438-8677.2011.00467.x, 2012.
- 740  
741 Harris, I., P. D. Jones, T. J. Osborn, and D. H. Lister: Updated high-resolution grids of monthly  
742 climatic observations - the CRU TS3.10 Dataset, *Int. J. Climatol.*, 34(3), 623-642,  
743 doi:10.1002/joc.3711, 2014.
- 744  
745 Hartmann, H., Adams, H. D., Hammond, W. M., Hoch, G., Landhäusser, S. M., Wiley, E. and  
746 Zaehle, S.: Identifying differences in carbohydrate dynamics of seedlings and mature trees to  
747 improve carbon allocation in models for trees and forests, *Environ. Exp. Bot.*, 152(September  
748 2017), 7–18, doi:10.1016/j.envexpbot.2018.03.011, 2018.
- 749  
750 Hartmann, H., Bahn, M., Carbone, M. and Richardson, A. D.: Plant carbon allocation in a  
751 changing world – challenges and progress: introduction to a Virtual Issue on carbon  
752 allocation: Introduction to a virtual issue on carbon allocation, *New Phytol.*, 227(4), 981–988,  
753 doi:10.1111/nph.16757, 2020.
- 754  
755 He, W., Liu, H., Qi, Y., Liu, F. and Zhu, X.: Patterns in nonstructural carbohydrate contents at the  
756 tree organ level in response to drought duration, *Glob. Chang. Biol.*, 26(6), 3627–3638,  
757 doi:10.1111/gcb.15078, 2020.
- 758  
759 Herrera-Ramírez, D., Muhr, J., Hartmann, H., Römermann, C., Trumbore, S. and Sierra, C. A.:



- 760 Probability distributions of nonstructural carbon ages and transit times provide insights into  
761 carbon allocation dynamics of mature trees, *New Phytol.*, 226(5), 1299 - 1311,  
762 doi:10.1111/nph.16461, 2020.
- 763
- 764 Hickler, T., Smith, B., Sykes, M. T., Davis, M. B., Sugita, S. and Walker, K.: Using a generalized  
765 vegetation model to simulate vegetation dynamics in northeastern USA, *Ecology*, 85(2), 519–  
766 530, doi:10.1890/02-0344, 2004.
- 767
- 768 Hoch, G., Richter, A. and Körner, C.: Non-structural carbon compounds in temperate forest trees,  
769 *Plant, Cell Environ.*, 26(7), 1067–1081, doi:10.1046/j.0016-8025.2003.01032.x, 2003.
- 770
- 771 Huang, J., Kautz, M., Trowbridge, A. M., Hammerbacher, A., Raffa, K. F., Adams, H. D.,  
772 Goodsmann, D. W., Xu, C., Meddens, A. J. H., Kandasamy, D., Gershenson, J., Seidl, R. and  
773 Hartmann, H.: Tree defence and bark beetles in a drying world: carbon partitioning,  
774 functioning and modelling, *New Phytol.*, 225(1), 26–36, doi:10.1111/nph.16173, 2020.
- 775
- 776 Hui, D., Deng, Q., Tian, H. and Luo, Y.: *Handbook of Climate Change Mitigation and Adaptation.*,  
777 2020.
- 778
- 779 IPCC: 2014: *Climate Change 2014: Synthesis Report. Contribution of Working Groups I, II and*  
780 *III to the Fifth Assessment Report of the Intergovernmental Panel on Climate Change*, edited  
781 by: Core Writing Team, Pachauri, R. K., and Meyer, L. A., IPCC, Geneva, Switzerland, 2014.
- 782
- 783 Jones, S., Rowland, L., Cox, P., Hemming, D., Wiltshire, A., Williams, K., Parazoo, N., Liu, J.,  
784 da Costa, A., Meir, P., Mencuccini, M. and Harper, A.: The Impact of a Simple Representation  
785 of Non-Structural Carbohydrates on the Simulated Response of Tropical Forests to Drought,  
786 *Biogeosciences Discuss.*, 1–26, doi:10.5194/bg-2019-452, 2019.
- 787
- 788 Kalnay, E., Kanamitsu, M., Kistler, R., Collins, W., Deaven, D., Gandin, L., Iredell, M.,  
789 Saha, S., White, G., Woollen, J., Zhu, Y., Chelliah, M., Ebisuzaki, W., Higgins, W.,  
790 Janowiak, J., Mo, K. C., Ropelewski, C., Wang, J., Leetmaa, A., Reynolds, R.,  
791 Jenne, R., & Joseph, D.: The NCEP/NCAR 40-Year Reanalysis Project, *Bulletin of*  
792 *the American Meteorological Society*, 77(3), 437-472. 1996
- 793
- 794 Klein, T. and Hoch, G.: Tree carbon allocation dynamics determined using a carbon mass balance  
795 approach, *New Phytol.*, 205(1), 147–159, doi:10.1111/nph.12993, 2015.



- 796  
797 Klein Tank, A.M.G. and Coauthors, 2002. Daily dataset of 20th-century surface air temperature  
798 and precipitation series for the European Climate Assessment. *Int. J. of Climatol.*, 22, 1441-  
799 1453.  
800  
801 Körner, C.: Carbon limitation in trees, *J. Ecol.*, 91(1), 4–17, doi:10.1046/j.1365-  
802 2745.2003.00742.x, 2003.  
803  
804 Krinner, G., Viovy, N., de Noblet-Ducoudré, N., Ogée, J., Polcher, J., Friedlingstein, P., Ciais, P.,  
805 Sitch, S. and Prentice, I. C.: A dynamic global vegetation model for studies of the coupled  
806 atmosphere-biosphere system, *Global Biogeochem. Cycles*, 19(1), 1–33,  
807 doi:10.1029/2003GB002199, 2005.  
808  
809 Landhäusser, S. M. and Lieffers, V. J.: Seasonal changes in carbohydrate reserves in mature  
810 northern *Populus tremuloides* clones, *Trees - Struct. Funct.*, 17(6), 471–476,  
811 doi:10.1007/s00468-003-0263-1, 2003.  
812  
813 Madani, N., Parazoo, N. C., Kimball, J. S., Ballantyne, A. P., Reichle, R. H., Maneta, M., Saatchi,  
814 S., Palmer, P. I., Liu, Z. and Tagesson, T.: Recent Amplified Global Gross Primary  
815 Productivity Due to Temperature Increase Is Offset by Reduced Productivity Due to Water  
816 Constraints, *AGU Adv.*, 1(4), doi:10.1029/2020av000180, 2020.  
817  
818 Martínez-Vilalta, J., Sala, A., Asensio, D., Galiano, L., Hoch, G., Palacio, S., Piper, F. I. and Lloret,  
819 F.: Dynamics of non-structural carbohydrates in terrestrial plants: A global synthesis, *Ecol.*  
820 *Monogr.*, 86(4), 495–516, doi:10.1002/ecm.1231, 2016.  
821  
822 McDowell, N., Pockman, W. T., Allen, C. D., Breshears, D. D., Cobb, N., Kolb, T., Plaut, J.,  
823 Sperry, J., West, A., Williams, D. G. and Yezzer, E. A.: Mechanisms of plant survival and  
824 mortality during drought: Why do some plants survive while others succumb to drought?,  
825 *New Phytol.*, 178(4), 719–739, doi:10.1111/j.1469-8137.2008.02436.x, 2008.  
826  
827 McDowell, N. G.: Mechanisms linking drought, hydraulics, carbon metabolism, and vegetation  
828 mortality, *Plant Physiol.*, 155(3), 1051–1059, doi:10.1104/pp.110.170704, 2011.  
829  
830 McDowell, N. G., Allen, C. D., Anderson-Teixeira, K., Aukema, B. H., Bond-Lamberty, B., Chini,  
831 L., Clark, J. S., Dietze, M., Grossiord, C., Hanbury-Brown, A., Hurr, G. C., Jackson, R. B.,



- 832 Johnson, D. J., Kueppers, L., Lichstein, J. W., Ogle, K., Poulter, B., Pugh, T. A. M., Seidl, R.,  
833 Turner, M. G., Uriarte, M., Walker, A. P. and Xu, C.: Pervasive shifts in forest dynamics in a  
834 changing world, *Science* (80-. ), 368(6494), doi:10.1126/science.aaz9463, 2020.  
835
- 836 Mitchard, E. T. A.: The tropical forest carbon cycle and climate change, *Nature*, 559(7715), 527–  
837 534, doi:10.1038/s41586-018-0300-2, 2018.  
838
- 839 Pan, Y., Birdsey, R. A., Fang, J., Houghton, R., Kauppi, P. E., Kurz, W. A., Phillips, O. L.,  
840 Shvidenko, A., Lewis, S. L., Canadell, J. G., Ciais, P., Jackson, R. B., Pacala, S. W.,  
841 McGuire, A. D., Piao, S., Rautiainen, A., Sitch, S., and Hayes, D.: A large and persistent  
842 carbon sink in the world’s forests, *Science* (1979), 333, 988–993,  
843 doi:10.1126/science.1201609, 2011.  
844
- 845 Rademacher, T., Fonti, P., LeMoine, J. M., Fonti, M. V., Basler, D., Chen, Y., Friend, A. D.,  
846 Seyednasrollah, B., Eckes-Shephard, A. H. and Richardson, A. D.: Manipulating phloem  
847 transport affects wood formation but not local nonstructural carbon reserves in an evergreen  
848 conifer, *Plant Cell Environ.*, 44(8), 2506–2521, doi:10.1111/pce.14117, 2021.  
849
- 850 Richardson, A. D., Carbone, M. S., Keenan, T. F., Czimczik, C. I., Hollinger, D. Y., Murakami, P.,  
851 Schaberg, P. G. and Xu, X.: Seasonal dynamics and age of stemwood nonstructural  
852 carbohydrates in temperate forest trees, *New Phytol.*, 197(3), 850–861,  
853 doi:10.1111/nph.12042, 2013.  
854
- 855 Sala, A., Woodruff, D. R. and Meinzer, F. C.: Carbon dynamics in trees: Feast or famine?, *Tree*  
856 *Physiol.*, 32(6), 764–775, doi:10.1093/treephys/tpr143, 2012.  
857
- 858 Sato, H. and Ise, T.: Effect of plant dynamic processes on African vegetation responses to climate  
859 change: Analysis using the spatially explicit individual-based dynamic global vegetation  
860 model (SEIB-DGVM), *J. Geophys. Res. Biogeosciences*, 117(3), 1–18,  
861 doi:10.1029/2012JG002056, 2012.  
862
- 863 Sato, H., Itoh, A. and Kohyama, T.: SEIB-DGVM: A new Dynamic Global Vegetation Model  
864 using a spatially explicit individual-based approach, *Ecol. Modell.*, 200(3–4), 279–307,  
865 doi:10.1016/j.ecolmodel.2006.09.006, 2007.  
866
- 867 Sato, H., Kobayashi, H., Beer, C. and Fedorov, A.: Simulating interactions between topography,



- 868 permafrost, and vegetation in Siberian larch forest, *Environ. Res. Lett.*, 15(9),  
869 doi:10.1088/1748-9326/ab9be4, 2020.
- 870
- 871 Sato, H., Kobayashi, H., Iwahana, G., and Ohta, T.: Endurance of larch forest ecosystems in  
872 eastern Siberia under warming trends, *Ecol. Evol.*, 6, 5690–5704,  
873 <https://doi.org/10.1002/ece3.2285>, 2016.
- 874
- 875 Seidl, R., Thom, D., Kautz, M., Martin-Benito, D., Peltoniemi, M., Vacchiano, G., Wild, J., Ascoli,  
876 D., Petr, M., Honkaniemi, J., Lexer, M. J., Trotsiuk, V., Mairota, P., Svoboda, M., Fabrika, M.,  
877 Nagel, T. A. and Reyer, C. P. O.: Forest disturbances under climate change, *Nat. Clim. Chang.*,  
878 7(6), 395–402, doi:10.1038/nclimate3303, 2017.
- 879
- 880 Sevanto, S.: Phloem transport and drought, *J. Exp. Bot.*, 65(7), 1751–1759,  
881 doi:10.1093/jxb/ert467, 2014.
- 882
- 883 Sevanto, S. and Dickman, L. T.: Where does the carbon go?-Plant carbon allocation under climate  
884 change, *Tree Physiol.*, 35(6), 581–584, doi:10.1093/treephys/tpv059, 2015.
- 885
- 886 Signori-Müller, C., Oliveira, R. S., Valentim Tavares, J., Carvalho Diniz, F., Gilpin, M., de V.  
887 Barros, F., Marca Zevallos, M. J., Salas Yupayccana, C. A., Nina, A., Brum, M., Baker, T. R.,  
888 Cosio, E. G., Malhi, Y., Monteagudo Mendoza, A., Phillips, O. L., Rowland, L., Salinas, N.,  
889 Vasquez, R., Mencuccini, M. and Galbraith, D.: Variation of non-structural carbohydrates  
890 across the fast–slow continuum in Amazon Forest canopy trees, *Funct. Ecol.*, 36(2), 341–355,  
891 doi:10.1111/1365-2435.13971, 2022.
- 892
- 893 Singh, K. P. and Srivastava, K.: Seasonal variation in the biomass and non-structural carbohydrate  
894 content of fine roots of teak (*Tectona grandis* L. f.) plantations in a dry tropical region, *Tree*  
895 *Physiol.*, 1(1), 31–36, doi:10.1093/treephys/1.1.31, 1986.
- 896
- 897 Smith, B., Prentice, I. C. and Sykes, M. T.: Representation of vegetation dynamics in the  
898 modelling of terrestrial ecosystems: Comparing two contrasting approaches within European  
899 climate space, *Glob. Ecol. Biogeogr.*, 10(6), 621–637, doi:10.1046/j.1466-  
900 822X.2001.00256.x, 2001.
- 901
- 902 Smith, M. G., Miller, R. E., Arndt, S. K., Kasel, S., and Bennett, L. T.: Whole-tree distribution  
903 and temporal variation of non-structural carbohydrates in broadleaf evergreen trees, *Tree*



- 904        *Physiol*, 38, 570–581, <https://doi.org/10.1093/treephys/tpx141>, 2018.
- 905
- 906        Stevens-Rumann, C. S., Kemp, K. B., Higuera, P. E., Harvey, B. J., Rother, M. T., Donato, D. C.,  
907        Morgan, P. and Veblen, T. T.: Evidence for declining forest resilience to wildfires under  
908        climate change, *Ecol. Lett.*, 21(2), 243–252, doi:10.1111/ele.12889, 2018.
- 909
- 910        Sveinbjörnsson, B., Smith, M., Traustason, T., Ruess, R. W. and Sullivan, P. F.: Variation in  
911        carbohydrate source-sink relations of forest and treeline white spruce in southern, interior and  
912        northern Alaska, *Oecologia*, 163(4), 833–843, doi:10.1007/s00442-010-1597-1, 2010.
- 913
- 914        Tei, S., Sugimoto, A., Liang, M., Yonenobu, H., Matsuura, Y., Osawa, A., Sato, H., Fujinuma, J.  
915        and Maximov, T.: Radial Growth and Physiological Response of Coniferous Trees to Arctic  
916        Amplification, *J. Geophys. Res. Biogeosciences*, 122(11), 2786–2803,  
917        doi:10.1002/2016JG003745, 2017.
- 918
- 919        Wang, Z., Zhou, Z. and Wang, C.: Defoliation-induced tree growth declines are jointly limited by  
920        carbon source and sink activities, *Sci. Total Environ.*, 762, 143077,  
921        doi:10.1016/j.scitotenv.2020.143077, 2021.
- 922
- 923        Watanabe, S., Hajima, T., Sudo, K. and Nagashima, T.: MIROC-ESM: model description and  
924        basic results of CMIP5-20c3m experiments, *Geosci. Model Dev. Discuss.*, 4(2), 1063–1128,  
925        doi:10.5194/gmdd-4-1063-2011, 2011.
- 926
- 927        Weedon, G. P., Balsamo, G., Bellouin, N., Gomes, S., Best, M. J., and Viterbo, P.: The WFDEI  
928        Meteorological Forcing Data, Research Data Archive at the National Center for  
929        Atmospheric Research, Computational and Information Systems Laboratory,  
930        <https://doi.org/10.5065/486N-8109>, 2018. Accessed 11 Dec 2020.
- 931
- 932        Woodruff, D. R. and Meinzer, F. C.: Water stress, shoot growth and storage of non-structural  
933        carbohydrates along a tree height gradient in a tall conifer, *Plant, Cell Environ.*, 34(11), 1920–  
934        1930, doi:10.1111/j.1365-3040.2011.02388.x, 2011.
- 935
- 936        Würth, M. K. R., Peláez-Riedl, S., Wright, S. J. and Körner, C.: Non-structural carbohydrate pools  
937        in a tropical forest, *Oecologia*, 143(1), 11–24, doi:10.1007/s00442-004-1773-2, 2005.
- 938
- 939        Xu, C., Liu, H., Anenkhonov, O. A., Korolyuk, A. Y., Sandanov, D. V., Balsanova, L. D.,





940 Naidanov, B. B. and Wu, X.: Long-term forest resilience to climate change indicated by  
941 mortality, regeneration, and growth in semiarid southern Siberia, *Glob. Chang. Biol.*, 23(6),  
942 2370–2382, doi:10.1111/gcb.13582, 2017.  
943  
944 Zheng, Y., Shen, R., Wang, Y., Li, X., Liu, S., Liang, S., Chen, J. M., Ju, W., Zhang, L. and Yuan,  
945 W.: Improved estimate of global gross primary production for reproducing its long-Term  
946 variation, 1982-2017, *Earth Syst. Sci. Data*, 12(4), 2725–2746, doi:10.5194/essd-12-2725-  
947 2020, 2020.  
948